Ab initio study of solute transition-metal interactions with point defects in bcc Fe

P. Olsson,[1] T. P. C. Klaver,[2] and C. Domain[1]
[1]*Département Matériaux et Mécanique des Composants (MMC), EDF-R&D, Les Renardières, F-77250 Moret sur Loing, France*
[2]*Department of Materials Science and Engineering, Delft University of Technology, The Netherlands*
(Received 22 June 2009; revised manuscript received 17 December 2009; published 2 February 2010)

The properties of 3*d*, 4*d*, and 5*d* transition-metal elements in α-Fe have been studied using *ab initio* density-functional theory. The intrinsic properties of the solutes have been characterized as well as their interaction with point defects. Vacancies and interstitials of ⟨110⟩ and ⟨111⟩ orientations have been considered in order to discern trends that may explain experimental evidence of solute influences on radiation response and possibly aid future material design regarding the choice of alloy composition. Depending on the solute element, the different interactions are governed by the chemical interactions and the solute size factor. It is shown that magnetic interactions play an important role for the properties of the center series 3*d* elements, especially so for the antiferromagnetically coupling V, Cr, and Mn. For the 4*d*, 5*d*, and remaining 3*d* elements the interaction with point defects is mainly governed by the solute size factor. The solute-solute interaction is mostly repulsive with a few exceptions. The interactions with vacancies are in most cases binding; but the second nearest neighbor configurations exhibit strong repulsion for the early transition metals. Cr and Mn interact strongly binding with interstitial defects. The trends of the solute defect interactions have been determined to depend on the characteristic local deformation. Early transition metals interact stronger with defects than late ones of equal size factor.

DOI: 10.1103/PhysRevB.81.054102 PACS number(s): 75.50.Bb, 61.72.J−, 71.15.Mb, 75.30.Hx

I. INTRODUCTION

Body-centered–cubic (bcc) iron alloys make up the base for the ferritic and ferritic/martensitic (F/M) steels which are used in many industrial applications and are especially useful in the nuclear industry where neutron radiation can aggressively degrade the material properties. In reactor pressure vessel ferritic steels, the solutes present have an influence on irradiation induced hardening and the embrittlement of the materials.[1] The point defects created by the neutron induced cascades are responsible for the diffusion of the solute atoms, leading to the formation of solute rich precipitates within the matrix. These clusters are enriched in Cu, Ni, Mn, Si, and P.[2,3] The presence of solute atoms also influences the formation of point defect clusters. Both the change in point defect clusters and the formation of solute rich clusters influence the mechanical properties of the steels. Furthermore, in order to reduce the activation of F/M steels, the substitution of easily activated solutes (e.g., Ni) by other transition metals (TMs) (e.g., W, Ta, and Mo) with the same macroscopic (e.g., mechanical and corrosion) properties is performed.[4] These solutes in solid solution are present in small amounts (few tenths of percent) and may interact also with point defects created under irradiation. The interactions of defects and solute elements play key roles in the evolution of the microstructure.

An example of radiation induced materials degradation, volumetric swelling, induced by fast neutrons[5] has since its discovery been successfully explained for some pure elements with phenomenological models. The main cause of neutron induced swelling seems to be the bias in the production of interstitial versus vacancy type clusters.[6] Large interstitial clusters, of which a fraction are glissile and diffuse one dimensionally, escape to sinks while vacancy clusters, which are essentially immobile, stay in the bulk of the grain where the neutron induced displacement cascades took place. For alloys the picture is more complicated and only recently have some advancements been made. A phenomenological model of the interstitial cluster diffusion in Fe-Cr has successfully explained some of the concentration dependency of the swelling under neutron irradiation.[7–12] The model used data from *ab initio* calculations,[13,14] which showed that a single ⟨111⟩ self-interstitial atom (SIA) has a strong long-ranged attractive interaction with solute Cr atoms along the line of compression (and glide). The SIAs in an $a/2\langle 111\rangle$ loop move independently, dragging the others along after they have moved.[15] As such, the interaction of a single ⟨111⟩ SIA with a solute atom is the first approximation of the true cluster-solute interaction. The effect of the attractive interaction between Cr atoms and SIAs on the Fe-Cr alloy is that the SIA loops feel the solute Cr as traps. As long as the density of traps increases, the rate of diffusion will decrease. This will bring the interstitial defect diffusion into the same time scale as the vacancy diffusion and will thus significantly increase recombination. When the solute density becomes high enough, the effective range of the traps will start to overlap and the trapping force will decrease again. It was shown, with the support of molecular-dynamics simulations on large simulation boxes, with an alloy cohesive model that closely fits the *ab initio* data,[16] that this model[7–9] of trapping in Fe-Cr reproduced the measured swelling minima at around 9 at. % Cr, assuming that the change in the rate of SIA loop diffusion is the main cause of the concentration dependency of swelling in Fe-Cr.

The relatively high interest of the self-interstitial defects in Fe is much due to the fact that Fe is special among the bcc metals in that the ⟨110⟩ self-interstitial is the most stable one by 0.7 eV with respect to the ⟨111⟩ self-interstitial.[14,17,18] A comparison of the SIA stability between all bcc metals has shown that it really is the ⟨111⟩ SIA in Fe, which behaves different from the expected trend.[19] The ⟨110⟩ SIA interac-

tion with solutes is an important factor for the evolution of the microstructure. However, for the special case of swelling, the three-dimensional character of the ⟨110⟩ migration[18] diminishes the long term significance of the ⟨110⟩ SIA-solute interaction.

Industrial ferritic (F/M) steels contain, in addition to Fe (Fe-Cr), many different transition metals in dilute concentration. Consequently the accurate characterization of the interaction of these solutes with point defects is of importance and can be investigated by *ab initio* calculations. Some of these TMs have already been studied, such as Cr,[14] Si, Mn, Ni, and Cu.[20,21] In fact, other elements than transition-metal impurities, such as C and N, are equally important in steels and Fe alloys and have been studied previously,[22] along with P.[23,24]

Here, we have performed a systematic theoretical study of the interactions between transition-metal elements and point defects in bcc Fe. The magnetic properties of substitutional transition-metal elements in Fe have been studied previously[25,26] for both the 3*d* and 4*d* rows. The importance of a correct description of the solute interaction with the host is crucial. This very basic parameter determines in many cases the character of the interactions of solute atoms with defects and is also used as a parameter in kinetic Monte Carlo simulations of processes such as thermal aging, solute segregation to the grain boundary, and volumetric damage accumulation.

II. METHOD OF CALCULATION

Four different density-functional theory (DFT) methods have been used:

(i) the commonly used ultrasoft pseudopotential (USPP) method of Vanderbildt;[27]

(ii) the more rigorous projector augmented wave (PAW) method,[28,29] both USPP and PAW as implemented in the Vienna *ab initio* simulation package (VASP) (Refs. 30–32);

(iii) full potential linearized augmented plane waves (LAPWs), as implemented in WIEN2K,[33] has been used for selected cases; and

(iv) the exact muffin-tin orbital (EMTO) method,[34] using the coherent potential approximation (CPA) (Ref. 35) for a mean-field approximation of chemical substitution, has been used as yet another approach, only for the intrinsic solution properties.

For the study with the PAW method, two different parametrizations of the generalized gradient approximation (GGA) have been used: that of Perdew and Wang (PW91) (Ref. 36) and that of Perdew-Burke-Ernzerhof (PBE).[37] For the spin interpolation of the correlation potential, both the standard one[38] and the improved Vosko-Wilk-Nusair (VWN) (Ref. 39) interpolation have been applied for the PAW and USPP methods within the PW91. It should be noted that in all instances where the PBE has been used, the VWN has been also applied. In all figures where only PAW or USPP is specified, it implies that the PW91 parametrization of the GGA has been used. For the bulk of the work, that is, the study of defect interactions with solute atoms, only the PAW method with the PW91 parametrization and the VWN interpolation has been used. For the LAPW calculations, the exchange correlation was treated using PBE and VWN. For the EMTO calculations, the PW91 and VWN were applied.

For the USPP and PAW calculations, supercells of 128 bcc positions were used with a Monkhorst-Pack $3\times3\times3$ *k*-point grid sampling the Brillouin zone. The plane wave expansions used in the USPP and PAW calculations were cut off at 300 eV. All relaxations were performed under constant volume conditions. For the LAPW calculations, supercells of 54 atoms were used with a $4\times4\times4$ *k*-point grid. For the EMTO calculation a CPA primitive cell was used with a 0.8% atomic concentration (in order to have the same solute concentration as in 128 atomic site supercells) of solutes with a $19\times19\times19$ *k*-point grid. The convergence of the parameters has previously been reported for the USPP,[17] PAW,[14] and EMTO (Ref. 40) methods. Moreover, a convergence test for the stability of the ⟨110⟩ SIA over the ⟨111⟩ SIA has been performed using simulation cells with 54 ($5\times5\times5$), 128 ($3\times3\times3$), 250 ($3\times3\times3$), 432 ($2\times2\times2$), and 1024 ($1\times1\times1$) lattice sites (*k*-points).

The local magnetic moments are calculated by taking the spin channel difference of the integrated charge density over the Wigner-Seitz sphere of the relevant atom. The substitution energy $E_s(M)$ of transition metal element M in Fe is defined in the extensive manner as

$$E_s(M) = E_{\text{tot}}(M) - (N-1)E_{\text{Fe}} - E_M, \tag{1}$$

where $E_{\text{tot}}(M)$ is the total energy of the system, N is the number of atoms, E_{Fe} is the Fe ground-state energy, and E_M is the M ground-state energy [for Cr, that of antiferromagnetic (AF) bcc]. The extensive definition thus represents the energy of substitution where a solution atom is taken from a reservoir and is well suited to determine substitution energies from supercell calculations. There is also an intensive definition of the substitution energy,

$$E_s(M) = \left.\frac{dH(c)}{dc}\right|_{c=0}, \tag{2}$$

where the enthalpy of formation $H(c)$ of the $\text{Fe}_{1-c}M_c$ alloy is defined as,

$$H(c_M) = E(\text{Fe}_{1-c}M_c) - [(1-c)E(\text{Fe}) + cE(M)]. \tag{3}$$

This definition is used when calculating the energy of substitution using a mean-field method like the CPA.

For the defect-solute and solute-solute interactions the binding energy of a configuration containing the objects A_i is defined as

$$E_b(A_1,A_2,\ldots,A_n) = \left[E\left(\sum A_i\right) + (n-1)E_{\text{ref}}\right] - \sum_i^n E(A_i), \tag{4}$$

where E_{ref} is the energy of the supercell without any objects, $E(A_i)$ is the energy of the supercell containing the single object A_i, and $E(\Sigma A_i)$ is the energy of the supercell containing all of the interacting objects. With this definition, negative values of E_b denote binding configurations.

The solute size factor of solute M in an Fe matrix is

TABLE I. Lattice parameter a_0 and magnetic moment μ of bcc Fe.

	USPP	USPP VWN	PAW	PAW VWN	LAPW	EMTO	Expt.[a]
a_0 (Å)	2.85	2.88	2.83	2.83	2.83	2.84	2.86
μ (μ_B)	2.35	2.48	2.17	2.21	2.21	2.20	2.22

[a]Reference 41.

$$\Omega_{\mathrm{sf}}^{M} = \frac{\Omega_M - \Omega_{\mathrm{Fe}}}{\Omega_{\mathrm{Fe}}} = \frac{1}{\Omega_{\mathrm{Fe}}}\frac{\partial \Omega}{\partial c}, \tag{5}$$

where c is the concentration of the solute and Ω is the volume and Ω_{Fe} is the atomic volume of bcc Fe. In a constant volume simulation, Ω_{sf}^{M} depends on the excess pressure induced by the solute in the host matrix. Via the bulk modulus, which relates the pressure and volume linearly,

$$B = -V\frac{\partial P}{\partial V}, \tag{6}$$

the size factor of solute M can be related to the excess pressure, ΔP, as

$$\Omega_{\mathrm{sf}}^{M} = -\frac{V}{\Omega_{\mathrm{Fe}} B}\Delta P. \tag{7}$$

The electronic charge density deformation map $\Delta\rho$ is defined by subtracting the electronic charge density $\rho(X_i)$ of each of the N individual atom X_i from the total charge density of the system ρ_{tot} considered as

$$\Delta\rho = \rho_{\mathrm{tot}} - \sum_{i}^{N} \rho(X_i). \tag{8}$$

In this study, over 400 self-consistent relaxation calculations were performed on supercells of 128 atomic sites.

III. RESULTS

Predicted equilibrium properties of pure bcc Fe from the different methods are listed in Table I. There are in general no significant differences in the predicted results between the methods except for the overestimation of the magnetic moment by the USPP method. The GGA lattice parameter for iron is slightly underestimated. The choice of PBE or PW91 does not significantly influence the predicted lattice parameter or magnetic moment.

The convergence with respect to the simulation box size for self-interstitial atoms, shown in Table II, validates the choice of box size for this study. Even at 54-lattice site simulation boxes ($3\times3\times3$ cubic bcc cells) the total energy difference between the $\langle 110\rangle$ and the $\langle 111\rangle$ SIAs is converged to within 20 meV. Thus, the 128-lattice site supercell used for all defect and/or solute interactions is deemed large enough and no significant box size effects are expected *a priori*. Furthermore, this comparison shows that constant volume conditions do not affect significantly the relative energies, such as the here presented relative stability or the binding energies.

A. Substitution

Substitutional transition-metal elements in bcc Fe are magnetic. The early 3*d* metals, up to Mn couple AF with the host, while the later ones couple ferromagnetically (FM).[25] The precise prediction of local impurity moments by density-functional theory is clearly more problematic for the AF coupling elements than for the FM coupling ones, see Fig. 1. From the review of the magnetic moments of 3*d* and 4*d* solutes by Drittler *et al.*,[25] we see good agreement and can also use the experimental data presented in it to confirm that the PAW method better describes the physics than the USPP method does. The magnetic moment of solute Mn in bcc Fe is especially difficult to pin down. The energy landscape with respect to the local Mn moment is rather shallow.

The energy of substitution for 3*d* elements in bcc Fe, as predicted by PAW, USPP, EMTO, and LAPW, is presented in Fig. 2. The clear correlation here shown between the character of magnetic coupling and the trend of the energy of substitution can be described with a crude model taking into account the *d*-band occupancy and the magnetic coupling,

$$E_s = \alpha\frac{N_d^M - N_d^{\mathrm{Fe}}}{2} + \beta J, \tag{9}$$

where α and β are proportionality constants, J is +1 for AF coupling, −1 for FM coupling, and 0 for the host, and N_d^M is the *d*-band occupation for element M. The model, illustrated in Fig. 2 using $\alpha=\beta=1$ to demonstrate the tendency of magnetically determined coupling, is only valid for the 3*d* solutes that have, as solutes, intrinsic moments. For FM elements larger moments give lower substitution energies, while for AF elements smaller moments give lower substitution energies. All elements far from Fe are oversized, with a size proportional to the band filling (or unfilling). For the FM

TABLE II. Stability of the $\langle 110\rangle$ SIA with respect to the $\langle 111\rangle$ SIA for different simulation cell sizes using PAW-VWN.

Box size (No. of lattice sites)	54	128	250	432	1024
$E_{\mathrm{tot}}^{\langle 111\rangle} - E_{\mathrm{tot}}^{\langle 110\rangle}$ (eV)	0.72	0.71	0.69	0.70	0.68

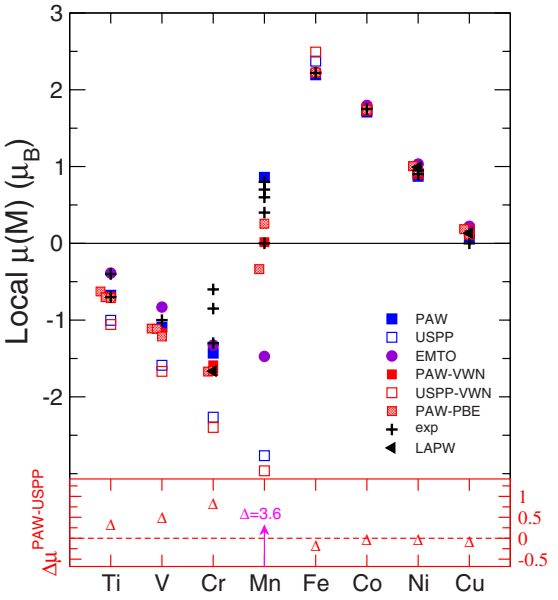

FIG. 1. (Color online) Top panel: Local magnetic moments of the substituted 3*d* elements in bcc Fe using different methods. The experimental data are from Refs. 42–51. The symbols slightly displaced from the exact positions along the abscissa represent results including semicore electrons in the valence while the undisplaced ones represent results using standard pseudopotentials. Bottom panel: difference in predicted moment (in μ_B) between the PAW and USPP methods.

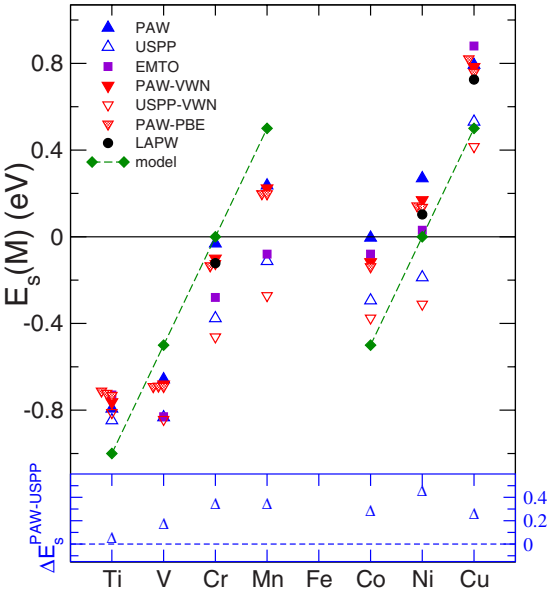

FIG. 2. (Color online) Top panel: energy of substitution for the 3*d* elements in bcc Fe using different methods. The symbols slightly displaced from the exact positions along the abscissa represent results including semicore electrons in the valence while the undisplaced ones represent results using minimal valence pseudopotentials. The model described by Eq. (9) is given by the diamonds connected by dashed lines. Bottom panel: Difference in predicted E_s (in eV) between the PAW and USPP methods.

coupling ones, the magnetic coupling is in competition with the effect of the decreasing volume since smaller volumes generally favor AF coupling. Consequently, the AF coupling oversized elements are *a priori* favorable in substitution.

For the model E_s prediction, Mn has been considered as AF, despite the small FM moment predicted by PAW, because an AF configuration on Mn is found for most of the defect configurations studied, coherent with the early TM position of Mn.

For the early 3*d* elements, which couple antiferromagnetically to the host, the difference between the USPP and PAW methods is consistently proportional to the *d*-band filling (see the bottom panels of Figs. 1 and 2). The main caveat of the USPP is its inability to correctly describe the strongly varying core part of the valence *d*-like orbitals and hence a divergence between the two methods is expected. The results are independent on the choice of GGA parametrization, but the inclusion of VWN interpolation of the spin polarization for the correlation term is important, especially so for the USPPs. The inclusion of semicore states introduces no significant changes in the here calculated properties. For the late 3*d* elements, which couple ferromagnetically to the host, the difference between the results of the two pseudopotential methods should decrease as a function of the *d*-band filling but not necessarily by a trivial negative proportionality since the core parts of the paired electrons will also contribute to the difference. As can be seen in the bottom panel of Fig. 2, Ni diverges from the trend. The USPP method incorrectly predicts a high local occupation at the Fermi level in the minority spin channel for the Ni atom. Thus the difference between the PAW and USPP predictions is due to a superposition of the effects of differently treated core parts of the *d*-electron wave functions as well as a shift of the minority spin band between the methods. For PAW, and as well LAPW, the Fermi energy lies in the second peak in the minority spin channel, thus raising the energy as compared to the USPP, which predicts the peak to be completely unoccupied, see Fig. 3. For Cu the difference in the predictions of the two methods is especially interesting since pure Cu is

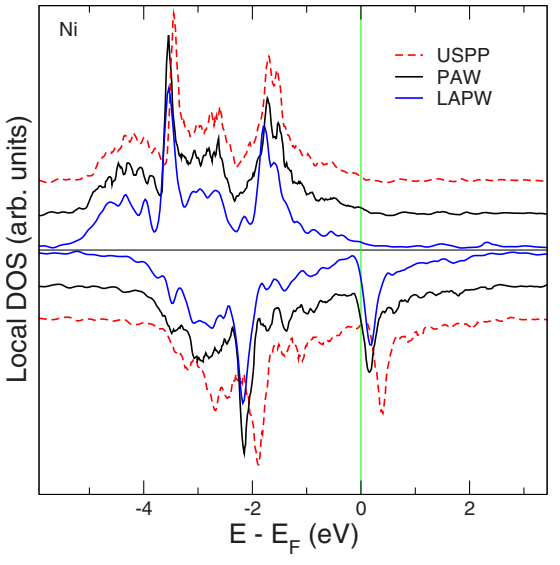

FIG. 3. (Color online) The local density of states for the Ni solute in an Fe matrix using the USPP-VWN, PAW-VWN, and LAPW methods. The curves are shifted in y for clarity.

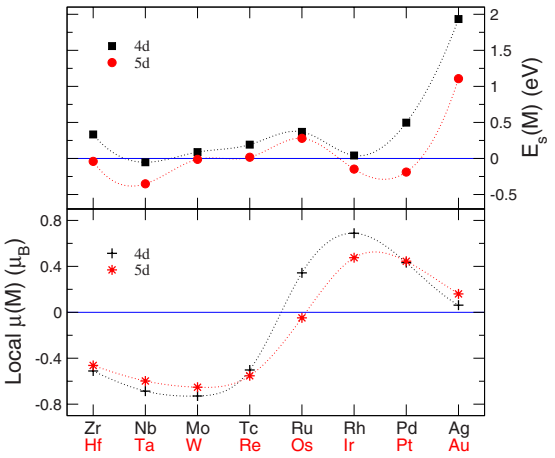

FIG. 4. (Color online) Top panel: energy of substitution for 4*d* and 5*d* elements calculated using PAW-VWN. Bottom panel: local magnetic moments for the substituted 4*d* and 5*d* elements.

one of the elements that most methods tend to handle well. Due to a fortuitous cancellation of errors in this case, the USPP values of about 0.5 eV (Ref. 17) are in better agreement with the experimental phase diagram than the PAW values are.

Only three cases have been studied using the LAPW method due to its relatively high-computational cost. These cases were chosen because they constitute important differences between the results of the two pseudopotential methods. Cr was chosen because of its technological interest and the rather significant difference in the heat of solution that does affect the interaction with defects.[14,52,53] Ni was chosen as a representative case where the USPP and PAW methods disagree on the sign of the energy of substitution. There seemed to be no connection between the dispersion in the predicted local Ni moment and the energy of substitution. Cu was chosen since the difference between the methods was uncharacteristically large. As can be clearly seen in Figs. 1 and 2, the LAPW predictions support the PAW results in all studied cases. For these results, between the PW91 and PBE parametrizations, there are no significant differences.

The EMTO method with CPA disorder has been added as a further point of reference since the local relaxation effects for substitutional impurities only weakly contribute to the solute interaction with the host. All 3*d* elements are oversized in Fe, even though most, except for Ti and Cu, are of comparative size with the host matrix.[54] Thus, one may expect that the effects of local relaxations will not be too severe. As has been deduced from unrelaxed PAW calculations and as can be seen from the EMTO results, this assessment is correct. The predicted EMTO local moments more or less follow the PAW predictions, although with a slight underestimation for the antiferromagnetically coupled elements. The case of largest discrepancy is for Mn, where the EMTO method predicts an AF moment as well as a negative energy of substitution, more in line with the USPP than the PAW. For calculating defect interactions with strong local relaxations, the EMTO-CPA approach is suboptimal in its current implementation and it is thus, only used in the current section.

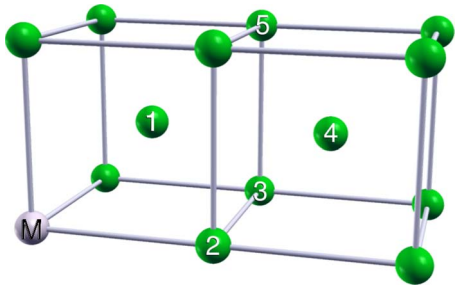

FIG. 5. (Color online) Solute-solute configurations. The first- to fifth-nearest-neighbor (1nn to 5nn) positions relative to the solute M in the bcc lattice.

The 4*d* and 5*d* elements are slightly magnetized by the host material in the manner expected from band filling arguments (see Fig. 4). Only the PAW-VWN results are shown. With respect to the 3*d* elements in substitution, the shift between AF and FM couplings is slightly shifted to the right; rendering Os a very weakly antiferromagnetically coupling impurity while Ru is weakly ferromagnetically interacting. In general the 4*d* elements have a strong tendency to phase separate in Fe.

B. Solute-solute interaction

From here on, all results are those predicted by the PAW method using VWN interpolation in the PW91 parametrization since it is the best compromise between computation speed and accuracy. Figure 5 displays the first to fifth nearest neighbor (1nn to 5nn) positions in the bcc matrix. We have investigated the interaction between the TM solute pairs in this range. Figure 6 displays the interaction strength of the solute pairs, from first to fifth nearest-neighbor positions. USPP results[20] are only in agreement with the PAW results here presented for the case of Cu. For Mn and Ni the trends are inversed with respect to PAW. The correlation between the solute-solute interaction and the energy of solution is not always straight forward. Note the case of Ni, for example,

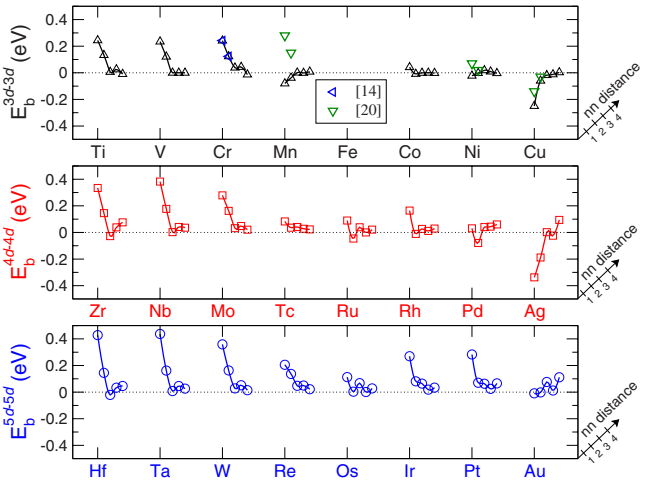

FIG. 6. (Color online) Solute-solute interaction for TM in Fe. The binding energy of first- to fifth-nearest-neighbor pairs is displayed.

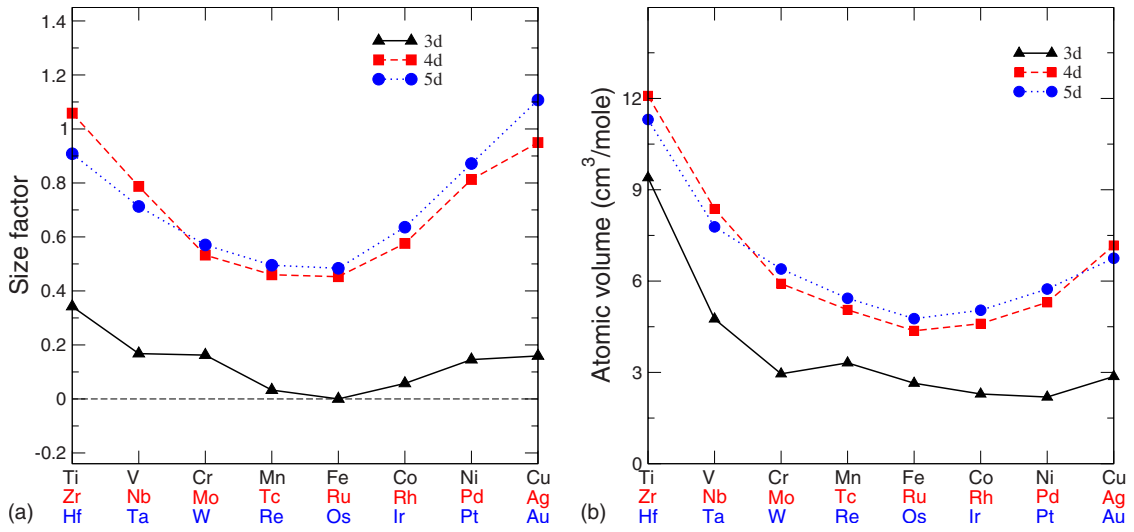

FIG. 7. (Color online) (a) Left panel: the predicted size factors of solute 3*d* (triangles), 4*d* (squares), or 5*d* (circles) atoms in a simulation cell of 128 atoms. (b) Right panel: the measured atomic volume of the 3*d* (triangles), 4*d* (squares), or 5*d* (circles) pure elements from Ref. 55.

where the positive energy of solution would suggest a tendency for phase separation, while there is no attraction between pairs of Ni atoms in the dilute limit. The conclusions drawn from taking only the solution energy into account is in disagreement with the Fe-Ni phase diagram. This issue is solved by observing the actual Ni-Ni interaction. In more concentrated alloys, neither value is expected to be valid since the screening from the alloy background comes into play. From Fig. 6 we see that the only elements that have local clustering tendencies, albeit in the dilute limit and at zero Kelvin, are Mn, Cu, and Ag. It is well known that Cu and Ag precipitate strongly in Fe. For the few solutes with self-attractive interaction energies, very small solute clusters in dilute iron alloys could thus appear. A consequence of these binding energies is in the solute atom effect on the defect migration since defect migration can strongly depend on the local environment.

C. Solute-defect interactions

The interaction between solutes and defects in a host matrix can have different components. The strain relief, based on the interaction of the strain field around a defect and the size factor of the solute is often a reasonable starting point. The strain fields are easy to calculate and the size factors of most solutes in Fe are published.[54] However, the chemical effect is more often than not the dominating factor. Furthermore, the size factor is determined by the chemistry. To distinguish chemical and pure strain relief effects is not straightforward. In addition, the published size factors[54] were measured at high concentrations and they seldom stem from the effects of the single solutes. In order to better approximate the single solute effect, one can relate its size factor to the pressure induced by a solute in substitution as per Eqs. (5)–(7). An oversized (undersized) solute is bound (repulsed) in tensile regions while repulsed (bound) in compressive ones. The strength of the interaction due to strain relief between a solute and a defect is to a first approximation proportional to the size factor. The size factor dependence on the chemistry is given by the *d*-band occupation and by the principal quantum number, much like the equilibrium volume dependence on the *d*-band occupation.[55] This isotropic approximation is rather crude, but still gives a good indication of the relative roles of size factor and thus chemically based or magnetically based interactions. In Fig. 7(a) the predicted size factors for the different transition metals as single solutes in a 128 atom simulation cell is shown. The size factors follow remarkably closely the atomic volume trend,[55] shown in Fig. 7(b). The most notable exception is for the 3*d* elements, where the magnetic effect (i.e., the TM-Fe chemical interaction) plays a much larger role than for the 4*d* and 5*d* elements. In general, the size factors of the late elements are higher than what would be elucidated from the volume variation; there is a tilting between the two figures. Even the fact that the two first 4*d* elements (Zr and Nb) are bigger than their 5*d* counterparts (Hf and Ta) is reproduced in the solute size factors. However, the same is not true for Ag and Au. These offsets are due to additional effects of the chemical interaction of the TM with the Fe matrix.

1. Solute-vacancy interactions

In Fig. 8 the binding energies of TM solutes with a single vacancy are displayed, for interaction distances of first- to fifth-nearest neighbors, as displayed in Fig. 5. The elements of the 5*d* and 4*d* row interact mainly through strain relief with vacancies: there is an attractive (repulsive) vacancy-solute interaction due to the compression (tension) character of the 1nn, 3nn, and 5nn (2nn, 4nn) configurations and due to the oversized character of these solutes. However, for the late elements, the vacancy is bound in all configurations while one would expect it to be repulsed as second nearest neighbor. Similar results are found in the literature using both USPP (Refs. 20 and 56) and PAW (Refs. 14 and 57) for some of the TM solutes. Also measurements[58,59] of the vacancy-

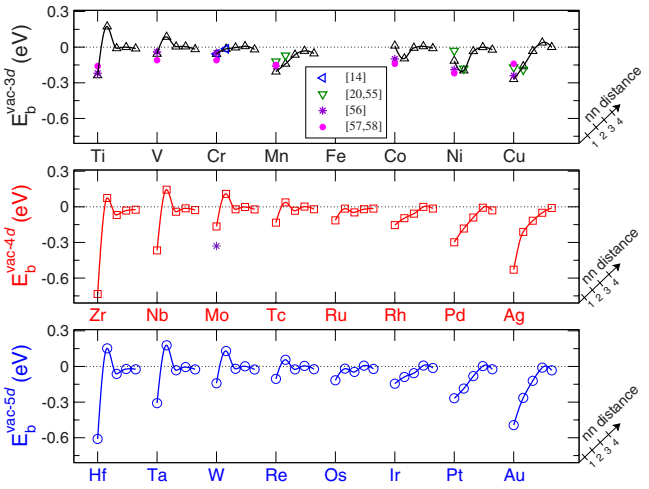

FIG. 8. (Color online) Solute-vacancy binding energies for 3*d* (top panel), 4*d* (middle panel), and 5*d* (bottom panel) elements for 1nn to 5nn relative positions.

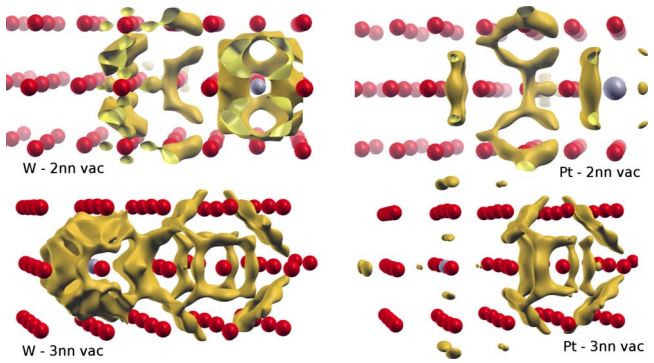

FIG. 9. (Color online) Charge density difference isosurfaces for W and Pt with a vacancy in 2nn (top) and 3nn (bottom) configurations. The red balls are Fe atoms and the blue ball is the solute. The vacancy is in the center of the cage structure.

solute interaction are in agreement with these results, although the measurements do not distinguish between first- and second-nearest-neighbor configurations. Also, for V and Cr, the measurements shown in Fig. 8 represent the upper (negative) bound on the interaction energy.

The relaxation of the nearest neighbor shells around a vacancy in Fe is Friedel-like, that is, they oscillate as compression, tension, compression. Table III shows the atomic relaxation in Fe predicted by PAW in a 128 atom simulation cell at constant volume.

The divergence for the second-nearest-neighbor interaction from the general trend cannot be explained either by the local magnetic moments, which vary only slightly depending on the vacancy position, nor the local density of states on the neighbor atoms. However, when examining the difference in charge density of these configurations with the superposition of the respective free atoms [Eq. (8)], one sees a significant difference in the behavior between the early and late TM solutes (see Fig. 9).

Around a vacancy in Fe there is a charge localization cage which, if disturbed by, for example the presence of a solute, can influence the binding energy. For the first nearest neighbors, the cages are strongly perturbed for all elements, but this effect is more than compensated for by the strong strain relief. For the third, and further, nearest neighbors, the vacancy charge cages are essentially unperturbed for all elements. The only clear difference is seen for the early TM solutes in second nearest-neighbor configuration. For the late element Pt in 2nn configuration, shown in Fig. 9, the shape of the cage differs only little from the unperturbed cage. For the early W in 2nn configuration, several features of the cage shape are modified. This charge cage perturbation gives rise to the repulsive interaction for the early TM solutes in 2nn position, seen in Fig. 8. The late elements are consistently bound in all positions.

The 3*d* elements show a much more complicated behavior due to the stronger magnetic coupling of the elements close around Fe in the row. The lightest ones, Ti and V, display the expected AF behavior, similar to the 4*d* and 5*d* elements of comparable sizes. The same is true for the FM interaction of Cu. For the intermediate 3*d* elements, the significant magnetic effect changes the character of the vacancy-solute interaction. That Cr is non-interacting should be expected since it is rather closely size matched with the matrix, which is also the case for Co. Mn is the only 3*d* element that has a strongly diverging character of interaction.[20] Its significant binding interaction is rather long ranged, reaching as far as the third nearest neighbor, considering that it is relatively well size matched. Mn interactions are influenced by its AF character when in proximity of a defect ($\mu_{\mathrm{Mn}}^{1nn}=-2.76\mu_B$ and $\mu_{\mathrm{Mn}}^{2nn}=-2.20\mu_B$) compared to in substitutional configuration ($\mu_{\mathrm{Mn}}^{subs}=+0.02\mu_B$).

2. *Solute-⟨110⟩ self-interstitial interactions*

The interaction between ⟨110⟩ interstitials with solute impurities has been studied in order to better interpret the nature of single interstitial diffusion in Fe based alloys. Figure 10 displays the considered configurations, where the solute atom is in close proximity to the interstitial defect.

Oversized solutes are expected to repulse the defect in the mixed (*M* in Fig. 10) and compressive configurations (*C* in Fig. 10), while attract the defect in the tensile configuration

TABLE III. The predicted relaxation of the neighbors around a vacancy in bcc Fe. The relaxation is given in percent of the first nearest-neighbor distance (2.452 Å).

Neighbor shell (nn)	1	2	3	4	5
Unrelaxed distance (Å)	2.452	2.831	4.004	4.695	4.903
Relaxation (%)	−3.40	+1.02	−0.606	−0.235	−0.223

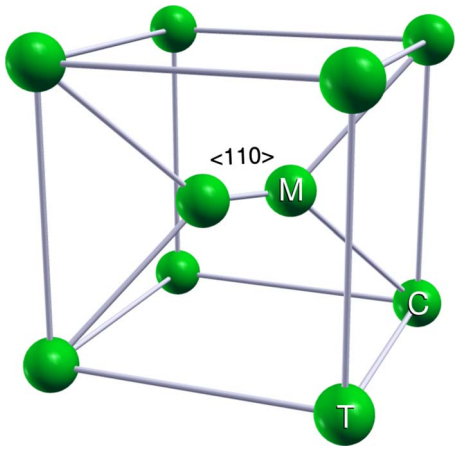

FIG. 10. (Color online) Solute-⟨110⟩ configurations. The letters *M* (mixed), *C* (compressed), and *T* (tensile) denote the position of the solute in the bcc Fe matrix with respect to a dumbbell.

(*T* in Fig. 10). From undersized solutes the inverse behavior is expected.

The solute-⟨110⟩ interaction is consistently repulsive in the mixed configuration except for Cr and Mn, see Fig. 11. For the 4*d* and 5*d* elements the repulsion is expected due to their oversized character but in the 3*d* row it is not as straightforward. For Cr and Mn this binding provides a possible interstitial mechanism for solute diffusion under irradiation. As opposed to the case of vacancy driven diffusion, there is no need for a 2nn binding energy in order to have drag. Mixed interstitials can lead to solute diffusion if they have a binding energy and if the barrier of interstitial migration is lower or equal to the SIA migration energy in the matrix. For both Mn (Ref. 21) and Cr (Ref. 53) this is the case. The strong binding interaction of Mn has been validated using kinetic Monte Carlo simulation[60] of isochronal annealing, which compare well with experiments.[61] The binding interaction of Cr has been validated by comparing molecular-dynamics simulations[12] with resistivity recovery

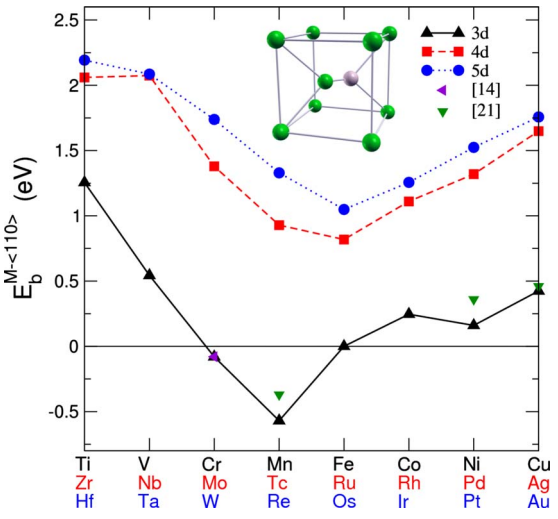

FIG. 11. (Color online) Solute *M*-⟨110⟩ mixed interstitial binding energy for 3*d* (triangles), 4*d* (squares), and 5*d* (circles) elements. The solute is inside the self-interstitial (see inset).

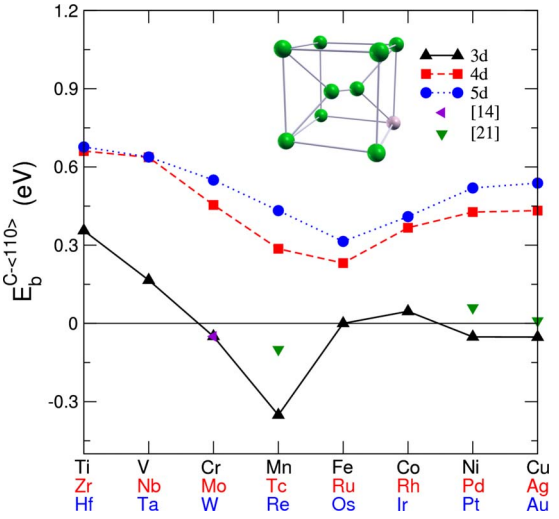

FIG. 12. (Color online) Solute *C*-⟨110⟩ interstitial binding energy for 3*d* (triangles), 4*d* (squares), and 5*d* (circles) elements. The solute is in the compression zone (see inset).

experiments.[62,63] There is a good agreement between USPP[21] and PAW results. The results of[64] are not included in Fig. 11 since they must be incorrectly calculated for the there included 4*d* and 5*d* solutes.

The solute-⟨110⟩ interaction is mostly repulsive in the compressed configuration except notably for Mn, but also weakly for Cr, Ni, and Cu (see Fig. 12). For the 4*d* and 5*d* elements the repulsion is expected due to their oversized character. Again the behavior of the 3*d* elements deviates from what the strain relief argument would lead us to expect. The general trend is similar to that of the mixed interstitial configuration, although somewhat damped since the compression is smaller in the compressed than in the mixed configuration. The agreement between the USPP (Ref. 21) and PAW results is weaker than that for the mixed SIA configurations.

For the tensile configuration, the solute-⟨110⟩ interaction is generally weaker and mostly attractive, see Fig. 13. The 4*d* and 5*d* elements all act as expected. Of the 3*d* elements, V is noninteracting; Cr and Co are slightly repulsive though they should all be weakly attracted according to strain relief. This configuration is the one with the largest difference between the USPP (Ref. 21) and PAW results, especially so for Mn. The binding interaction of Cu in the tensile configuration has been shown to give a correct interpretation[60] of the effect of the Cu concentration in isochronal annealing experiments.[65]

3. Solute-⟨111⟩ self-interstitial interactions

The interaction distance and strength between a ⟨111⟩ self-interstitial (or crowdion) and a solute M has been investigated in order to elucidate the different patterns of interstitial loop migration in Fe with transition-metal impurities. The ⟨111⟩ self-interstitial is unstable in Fe, but large interstitial clusters can be arranged as a collection of ⟨111⟩ SIA to form $a/2\langle 111\rangle$ interstitial loops. Figure 14 displays the shells that atoms along the ⟨111⟩ line can occupy.

The interaction is weak and short ranged for most of the 3*d* elements (see Fig. 15). Ti, Mn and Cr are the main ex-

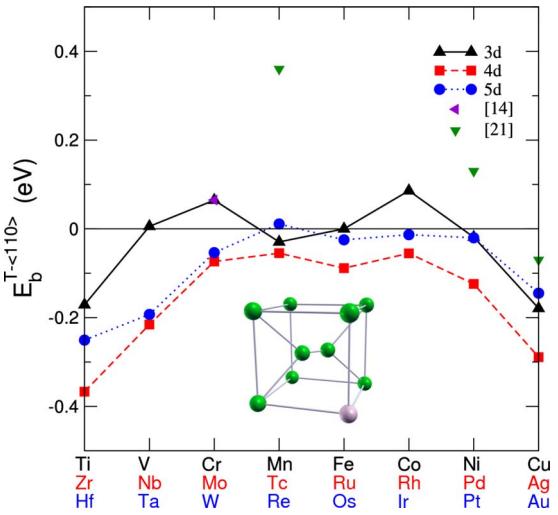

FIG. 13. (Color online) Solute T-⟨110⟩ interstitial binding energy for 3d (triangles), 4d (squares), and 5d (circles) elements. The solute is in the tensile zone (see inset).

ceptions. For Cr, the interaction distance is on the order of a nanometer and the maximum attractive interaction is −0.4 eV. For Mn, the distance is the same as for Cr but the maximum attractive interaction is larger, up to −0.7 eV. Ti has the same distance but with a repulsive interaction with a maximum energy of 0.5 eV. V is a particular case as it is rather strongly repulsed in a ⟨110⟩ interstitial but almost noninteracting with the ⟨111⟩ defect. Ni and Cu are stable only in first shell positions from the defect center. For most 3d elements the interaction vanishes from the third shell (3s position in Fig. 14) along the ⟨111⟩ line. Therefore, one can estimate the length of the crowdion itself as being twice the third shell distance, which amounts to about 0.14 nm in bcc Fe. This estimate can be further discussed by looking at how localized the crowdion is (see Fig. 16). The pure crowdion is rather localized in Fe and the mixed crowdions, although slightly less localized, do not diverge strongly from the pure Fe behavior.

The local relaxation around the 0s position (mixed crowdion, see Fig. 14) is strongly linked to the character of the interaction (see Fig. 16). The binding solutes (V, Cr, Mn) only slightly perturb the shape of the crowdion, while the repulsed solutes expand the crowdion. Also the magnetic coupling plays a significant role. An AF coupling element perturbs the crowdion less than an FM coupling of the same size does.

The 4d and 5d elements are strongly repulsed by the ⟨111⟩ interstitial, more so for the FM- than for the AF coupling ones. They are all greatly oversized elements and repulse the highly mobile interstitial defect to such an extent that it is very difficult to perform a similar study for the 4d and 5d elements to that shown in Figs. 15 and 16 for the 3d elements. During the ionic relaxation the defect is simply pushed away to the farthest point possible in the supercell. One might think to circumvent this problem by using noncubic supercells but then the intrinsic metastability of the ⟨111⟩ defect with respect to the ⟨110⟩ causes a spontaneous change of direction, unless unphysical constraints are introduced.

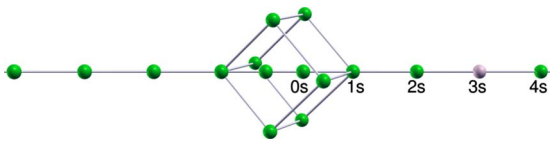

FIG. 14. (Color online) Solute M-⟨111⟩ interstitial interaction along the ⟨111⟩ line. In this example the solute M is in the third shell. N_s is the nth shell position for the solute M.

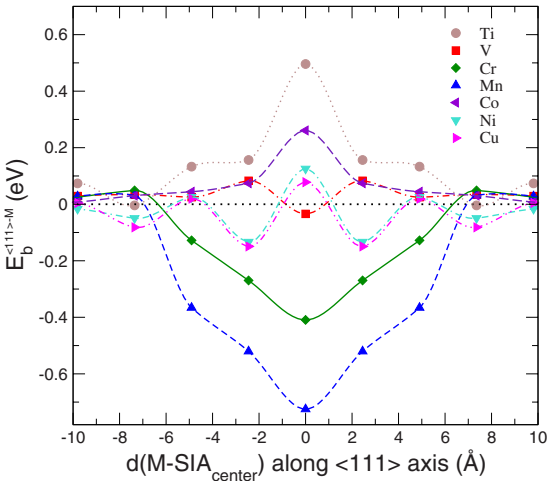

FIG. 15. (Color online) Solute 3d-⟨111⟩ interstitial binding energy of configurations with the solute at different positions along the ⟨111⟩ line.

IV. DISCUSSION

It is clearly seen when comparing the self interstitial-solute interactions (Figs. 11–13) with the size factors (Fig. 7) that the interaction between solute and interstitial defect is for a majority of the elements well described as being due to the size factor. A comparison between the data in Figs. 8

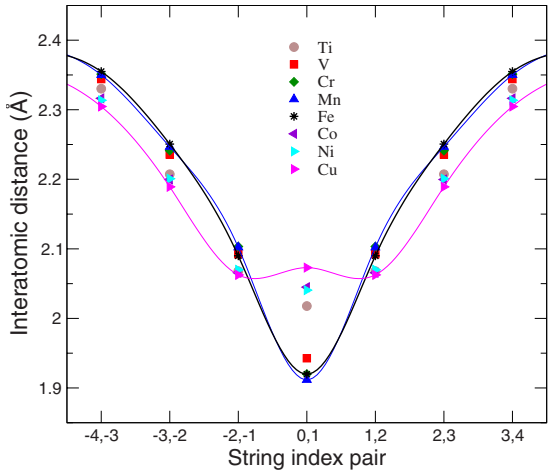

FIG. 16. (Color online) The interatomic distances between pairs of atoms along the ⟨111⟩ string with a solute M in the center of the crowdion (0s position). The reference case Fe and the two limiting cases Cu and Mn are traced by solid lines.

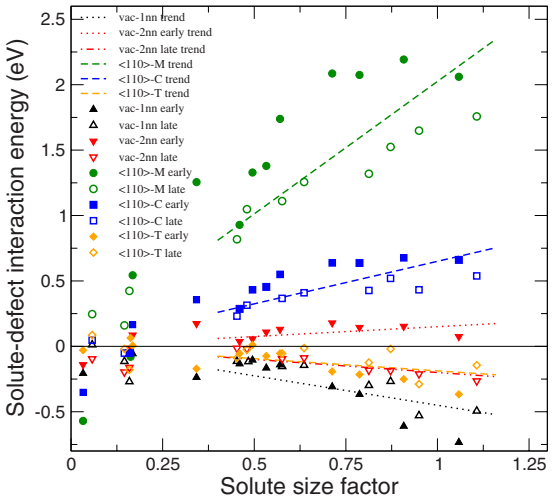

FIG. 17. (Color online) The solute-defect interaction energy as a function of solute size factor. The vacancy-1nn early/late solute (black filled/unfilled up triangle), the vacancy-2nn early/late solute (red filled/unfilled down triangle), the ⟨110⟩-*M* early/late (green filled/unfilled circle), the ⟨110⟩-*C* early/late (blue filled/unfilled square) and the ⟨110⟩-*T* early/late (orange filled/unfilled diamond) are represented. Linear regressions are shown to indicate the different trends (see text for analysis).

(first and second nn solute-vacancy interactions) and Figs. 11–13 (solute-SIA interactions) with respect to the size factor is shown in Fig. 17.

The evolution of these different interaction energies is proportional to the size factor (relation given by the interaction coefficient γ). The γ evolution for the different sites (*M*, *C*, *T*, 1nnV, and 2nnV) is related to the local perturbation of the sites. Table IV gives the local atomic displacements and γ.

Several trends can be distinguished:

(i) the solute *M*-⟨110⟩ interaction has the steepest repulsion (γ=2.03 eV);

(ii) the solute *C*-⟨110⟩ interaction has a less steep repulsion (γ=0.65 eV);

(iii) the repulsive vacancy-2nn early TM solute interaction (γ=0.15 eV);

(iv) the attractive solute *T*-⟨110⟩ interaction (γ =−0.188 eV);

(v) the attractive vacancy-2nn late TM solute interaction (γ=−0.2 eV); and

(vi) the attractive vacancy-1nn solute interaction (γ =−0.45 eV).

Furthermore, for all the different interaction sites, the early and late TM can be distinguished. For a given solute size factor, the interaction is stronger (attractive or repulsive) for early TM than for late TM.

The most notable exceptions from this interaction strength trend are, again, Cr and Mn, which strongly diverge due to their significant magnetic interactions with the defects.[14,20,21,52] These interactions override the repulsion due to their slightly oversized characters and bind the solute to the defect. For the 3*d* solutes, there is in fact a binding contribution proportional to the AF local moment of the solute atom.

In addition, Ti, although weakly magnetic and largely oversized, is more strongly repulsive/attractive than what these trends suggest. This is most probably due to the role of the delocalized *s*-electrons in Ti.

V. CONCLUSIONS

The energetic and magnetic properties of transition-metal solutes in bcc Fe have been investigated. Based on the predictions of the local magnetic moments and solute substitution energies, it is shown that the PAW method renders essentially the same results as the LAPW does and is also in agreement with the measured local magnetic moments from the literature. Therefore the PAW method should be the optimal choice when studying properties of magnetic transition metals in terms of accuracy and computational cost. Between PAW and USPP, for most of the cases where magnetic and electronic interactions are not predominant the difference is small and the trends are respected, but when these effects are large, such as for Mn, there is a large discrepancy.

The interaction between transition-metal atoms and point defects in bcc Fe is mostly governed by strain relief due to the size factor in the 4*d* and 5*d* rows. Vacancies are bound and interstitials are repulsed. The FM coupling 3*d* elements generally interact repulsively with interstitials and bind to vacancies. The interaction of the AF coupling 3*d* elements with point defects is markedly different. The strong magnetic coupling of the 3*d* elements close to the center of the period overrides the strain relief contribution to the interaction energy. Mn is the most strongly deviating element and binds both interstitials and vacancies, even though the Mn atom is slightly oversized. This is clearly due to electronic structure effects and closely linked to its half-filled *d* band. For the damage accumulation and recombination aspect, it is difficult to draw strong conclusions about Mn from this study since there is no great distinction in the interactions between the vacancy and interstitial type defects for Mn. However, the simple fact that interstitials are slowed down somewhat closes the gap in the mobility bias between interstitial and

TABLE IV. The local atomic displacement *u* is taken from relaxed defect configurations in pure Fe; the interaction coefficient γ for the different defect-solute configurations (*M*, *C*, *T*, 1nnV, and 2nnV)

Defect	⟨110⟩-*M*	⟨110⟩-*C*	⟨110⟩-*T*	1nn V	2nn V
u (Å)	+0.983	+0.333	−0.028	−0.083	+0.025
γ (eV)	+2.03	+0.65	−0.188	−0.45	+0.15 (late TM) −0.2 (early TM)

vacancy type clusters and an increased recombination should be seen in dilute Fe-Mn alloys, in agreement with experiments.[66] Solute Cr on the other hand binds only interstitials and should therefore significantly slow down the interstitial cluster diffusion while it is at the same time transparent to vacancies. The predictions of mixed Fe-Cr dumbbells are in agreement with experiments.[66,67] V is an interesting element since it is largely transparent to vacancies and also to the ⟨111⟩ type interstitials while it does, however, repulse rather strongly the ⟨110⟩ interstitials. Thus, one can expect to see differences for dilute Fe-V alloys in the single-interstitial diffusion pattern but not in that of interstitial loops, with respect to that in pure Fe.

The interactions with vacancies display quite regular trends over all the *d* series with one exception: the 2nn repulsion of the early TM (AF coupling) solutes. The increase in energy can be traced not to the AF coupling, but rather to the charge localization of the less than half-filled *d* band. The early TM elements strongly perturb the charge density around the vacancy in 2nn position, thus increasing the energy of the system, while the late TM solutes (FM coupling, more than half filled *d* band) do not. Solute diffusion through vacancy drag in bcc crystals can only occur if there is a binding interaction for the 1nn and the 2nn (or 3nn) configurations. Thus, solute diffusion by vacancy drag should not be expected for the early TM elements in Fe, except for Mn which exhibits consistent long range binding and for Zr and Hf, which have 3nn binding interactions.

Most of the interesting physics and most of the deviations from the strain relief model are present for strongly AF coupling solutes. For the self-interstitials, the attraction of oversized solutes is due to the magnetic coupling. Since the solute couples AF with the matrix atoms, the shorter bond lengths enforced by the self-interstitial do not frustrate the local magnetism as much as FM ones would, thus lowering the energy of the system. For the FM coupling solutes, no such lowering can take place as the frustration is essentially the same as in the pure Fe matrix.

It has been shown that all TM solutes interact with point defects and may affect the evolution of the microstructure under irradiation. For dilute solutes, only binding interactions will significantly affect the kinetics. For the interaction with self-interstitials, one of the three configurations (tensile, mixed dumbbell or compression) is always binding (except for Co and V). It is expected to the first order that the interaction between solutes and point defect clusters follow the same trends as for the single point defects.

Early TM solutes have larger interaction energies (positive or negative) than late TM solutes, when comparing equally oversized elements. Magnetic effects with AF or FM coupling explains some of the interactions obtained and are the consequence of the chemical interaction and the electronic structure effects. Nevertheless, these chemical effects do not always affect the magnetic properties, as has been shown for TM-vacancy interactions in 2nn position for example.

These data can be used to construct energetic models for larger scale simulations. It is, for example, possible to take advantage of the here presented systematic trends to build interatomic alloy potentials for classical molecular-dynamics simulations[68] or to derive cohesive models for kinetic Monte Carlo simulations.

ACKNOWLEDGMENTS

The authors acknowledge fruitful discussion with L. Malerba and D. Terentyev. This work was supported by the European Commission in the framework of the PERFECT IP under Contract No. FI6O-CT-2003-5088-40, as well as by Grant No. 212175 (GetMat project) and Grant No. 232612 (PERFORM60 project) in FP7/2007-2011. The calculations were partly performed on the supercomputers at Centre de Calcul Recherche et Technologie (CCRT) in the framework of an EDF-CEA contract.

[1] M. Lambrecht, L. Malerba, and A. Almazouzi, J. Nucl. Mater. **378**, 282 (2008).
[2] J. T. Buswell, W. J. Phythian, R. J. McElroy, S. Dumbill, P. H. N. Ray, J. Mace, and R. N. Sinclair, J. Nucl. Mater. **225**, 196 (1995).
[3] P. Auger, P. Pareige, S. Welzel, and J.-C. Van Duysen, J. Nucl. Mater. **280**, 331 (2000).
[4] B. van der Schaaf, D. S. Gelles, S. Jitsukawa, A. Kimura, R. L. Klueh, A. Möslang, and G. R. Odette, J. Nucl. Mater. **283-287**, 52 (2000).
[5] E. A. Little and D. A. Stow, J. Nucl. Mater. **87**, 25 (1979).
[6] B. N. Singh, S. I. Golubov, H. Trinkaus, A. Serra, Y. N. Osetsky, and A. V. Barashev, J. Nucl. Mater. **251**, 107 (1997).
[7] D. Terentyev, L. Malerba, and A. V. Barashev, Philos. Mag. Lett. **85**, 587 (2005).
[8] D. A. Terentyev, Ph.D. dissertation, Free University of Brussels, 2006 (http://www.sckcen.be/sckcen_en/publications/theses/PhD_Terentyev_v3_06112006.pdf).
[9] D. Terentyev, P. Olsson, L. Malerba, and A. V. Barashev, J. Nucl. Mater. **362**, 167 (2007).
[10] D. Terentyev, L. Malerba, and A. V. Barashev, Philos. Mag. **88**, 21 (2008).
[11] D. Terentyev, P. Olsson, and L. Malerba, J. Nucl. Mater. **386-388**, 140 (2009).
[12] D. Terentyev, P. Olsson, T. P. C. Klaver, and L. Malerba, Comput. Mater. Sci. **43**, 1183 (2008).
[13] P. Olsson, *Modelling of Formation and Evolution of Defects and Precipitates in Fe–Cr Alloys of Reactor Relevance—Acta Universitatis Upsaliensis* (Faculty of Science and Technology, Uppsala University, Sweden, 2005).
[14] P. Olsson, C. Domain, and J. Wallenius, Phys. Rev. B **75**, 014110 (2007).
[15] Y. N. Osetsky, D. J. Bacon, A. Serra, B. N. Singh, and S. I. Golubov, Philos. Mag. A **83**, 61 (2003).
[16] P. Olsson, J. Wallenius, C. Domain, K. Nordlund, and L. Malerba, Phys. Rev. B **72**, 214119 (2005); **74**, 229906(E) (2006).

[17] C. Domain and C. S. Becquart, Phys. Rev. B **65**, 024103 (2001).
[18] C. C. Fu, F. Willaime, and P. Ordejón, Phys. Rev. Lett. **92**, 175503 (2004).
[19] D. Nguyen-Manh, A. P. Horsfield, and S. L. Dudarev, Phys. Rev. B **73**, 020101(R) (2006).
[20] E. Vincent, C. S. Becquart, and C. Domain, J. Nucl. Mater. **351**, 88 (2006).
[21] E. Vincent, C. S. Becquart, and C. Domain, J. Nucl. Mater. **359**, 227 (2006).
[22] C. S. Becquart, C. Domain, and J. Foct, Philos. Mag. **85**, 533 (2005).
[23] C. Domain and C. S. Becquart, Phys. Rev. B **71**, 214109 (2005).
[24] E. Meslin, Chu-Chun Fu, A. Barbu, F. Gao, and F. Willaime, Phys. Rev. B **75**, 094303 (2007).
[25] B. Drittler, N. Stefanou, S. Blügel, R. Zeller, and P. H. Dederichs, Phys. Rev. B **40**, 8203 (1989).
[26] V. I. Anisimov, V. P. Antropov, A. I. Liechtenstein, V. A. Gubanov, and A. V. Postnikov, Phys. Rev. B **37**, 5598 (1988).
[27] D. Vanderbilt, Phys. Rev. B **41**, 7892 (1990).
[28] P. E. Blöchl, Phys. Rev. B **50**, 17953 (1994).
[29] G. Kresse and D. Joubert, Phys. Rev. B **59**, 1758 (1999).
[30] G. Kresse and J. Hafner, Phys. Rev. B **47**, 558 (1993).
[31] G. Kresse and J. Hafner, Phys. Rev. B **49**, 14251 (1994).
[32] G. Kresse and J. Hafner, J. Phys.: Condens. Matter **6**, 8245 (1994).
[33] P. Blaha, K. Schwarz, G. K. H. Madsen, D. Kvasnicka, and J. Luitz, *WIEN2k—An Augmented Plane Wave+Local Orbitals Program for Calculating Crystal Properties*, edited by K. Schwarz (Techn. Universtät, Wien, Austria, 2001).
[34] O. K. Andersen and T. Saha-Dasgupta, Phys. Rev. B **62**, R16219 (2000).
[35] L. Vitos, Phys. Rev. B **64**, 014107 (2001).
[36] J. P. Perdew, J. A. Chevary, S. H. Vosko, K. A. Jackson, M. R. Pederson, D. J. Singh, and C. Fiolhais, Phys. Rev. B **46**, 6671 (1992).
[37] J. P. Perdew, K. Burke, and M. Ernzerhof, Phys. Rev. Lett. **77**, 3865 (1996).
[38] U. von Barth and L. Hedin, J. Phys. C **5**, 1629 (1972).
[39] S. H. Vosko, L. Wilk, and M. Nusair, Can. J. Phys **58**, 1200 (1980).
[40] P. Olsson, I. A. Abrikosov, L. Vitos, and J. Wallenius, J. Nucl. Mater. **321**, 84 (2003).
[41] C. Kittel, *Introduction to Solid State Physics* (Wiley, New York, 1958).
[42] A. T. Aldred, B. D. Rainford, J. S. Kouvel, and T. J. Hicks, Phys. Rev. B **14**, 228 (1976).
[43] F. Kajzar and G. Parette, J. Appl. Phys. **50**, 1966 (1979).
[44] H. R. Child and J. W. Cable, Phys. Rev. B **13**, 227 (1976).
[45] I. Mirebeau, G. Parette, and J. W. Cable, J. Phys. F: Met. Phys. **17**, 191 (1987).
[46] M. F. Collins and G. G. Low, Proc. Phys. Soc. London **86**, 535 (1965).
[47] M. F. Collins and J. B. Forsyth, Philos. Mag. **8**, 401 (1963).
[48] P. Radhakrishna and F. Livet, Solid State Commun. **25**, 597 (1978).
[49] S. S. Shinozaki and A. Arrott, Phys. Rev. **152**, 611 (1966).
[50] C. G. Shull and M. K. Wilkinson, Phys. Rev. **97**, 304 (1955).
[51] Y. Nakai and N. Kunitomi, J. Phys. Soc. Jpn. **39**, 1257 (1975).
[52] T. P. C. Klaver, P. Olsson, and M. W. Finnis, Phys. Rev. B **76**, 214110 (2007).
[53] P. Olsson, J. Nucl. Mater. **386-388**, 86 (2009).
[54] H. W. King, J. Mater. Sci. **1**, 79 (1966).
[55] K. A. Gschneidner, Solid State Phys. **16**, 275 (1964).
[56] C. Domain, J. Nucl. Mater. **351**, 1 (2006).
[57] T. Ohnuma, N. Soneda, and M. Iwasawa, Acta Mater. **57**, 5947 (2009).
[58] M. Doyama, Trans. Jpn. Inst. Met. **25**, 808 (1986).
[59] A. Möslang, E. Albert, E. Recknagel, A. Weidinger, and P. Moser, Hyperfine Interact. **17-19**, 255 (1984).
[60] R. Ngayam-Happy, P. Olsson, C. S. Becquart, and C. Domain, J. Nucl. Mater. (unpublished).
[61] F. Maury, A. Lucasson, P. Lucasson, P. Moser, and Y. Loreaux, J. Phys. F: Met Phys. **16**, 523 (1986).
[62] A. Benkaddour, C. Dimitrov, and O. Dimitrov, Mater. Sci. Forum **15-18**, 1263 (1987).
[63] C. Dimitrov, A. Benkaddour, C. Corbel, and P. Moser, Ann. Chim. (Paris) **16**, 319 (1991).
[64] D. Nguyen-Manh, M. Yu. Lavrentiev, and S. L. Dudarev, J. Comp.-Aided, Mater. Des. **14**, 159 (2007).
[65] F. Maury, A. Lucasson, P. Lucasson, P. Moser, and F. Faudot, J. Phys.: Condens. Matter **2**, 9291 (1990).
[66] H. Abe and E. Kuramoto, J. Nucl. Mater. **271-272**, 209 (1999).
[67] F. Maury, P. Lucasson, A. Lucasson, F. Faodo, and J. Bigot, J. Phys. F: Met. Phys. **17**, 1143 (1987).
[68] D. J. Hepburn, G. J. Ackland, and P. Olsson, Philos. Mag. **89**, 3393 (2009).